Interplay of Andreev Reflection and Coulomb Blockade in Hybrid Superconducting Single-Electron Transistors

Laura Sobral Rey,[1] David Christian Ohnmacht,[1] Clemens B. Winkelmann,[2] Jens Siewert,[3,4] Wolfgang Belzig,[1] and Elke Scheer[1,*]

[1]Physics Department, University of Konstanz, 78457 Konstanz, Germany
[2]Université Grenoble Alpes, CNRS, Grenoble INP, Institut Néel, 38000 Grenoble, France
[3]University of the Basque Country UPV/EHU and EHU Quantum Center, 48080 Bilbao, Spain
[4]Ikerbasque, Basque Foundation for Science, 48009 Bilbao, Spain

(Received 11 May 2023; revised 29 August 2023; accepted 22 December 2023; published 2 February 2024)

We study the interplay between Coulomb blockade and superconductivity in a tunable superconductor–superconductor–normal-metal single-electron transistor. The device is realized by connecting the superconducting island via an oxide barrier to the normal-metal lead and with a break junction to the superconducting lead. The latter enables Cooper pair transport and (multiple) Andreev reflection. We show that these processes are relevant also far above the superconducting gap and that signatures of Coulomb blockade may reoccur at high bias while they are absent for small bias in the strong-coupling regime. Our experimental findings agree with simulations using a rate equation approach in combination with the full counting statistics of multiple Andreev reflection.

DOI: 10.1103/PhysRevLett.132.057001

Coulomb blockade (CB) is an archetypical manifestation of charge quantization (CQ), which occurs in the electronic transport across a small metallic island [1]. CB can be suppressed by both classical and quantum fluctuations of the charge [2]. Classical charge fluctuations originate from thermal activation over an energy barrier, provided by the charging energy $E_C = e^2/2C$, with C the total capacitance and e the elementary charge. The quantum fluctuations can be described using the Landauer-Büttiker picture using individual conductance channels $i = 1 \ldots M$, with transmissions $0 \leq \tau_i \leq 1$, connecting the island to the leads [2]. In the case of normal-metallic (N) leads, the magnitude of the conductance oscillations in a Coulomb-blockaded island in a single electron transistor (SET) [3,4] was predicted to scale like $\prod_i \sqrt{1-\tau_i} \exp(-k_B T/E_C)$ [5], which was shown to hold experimentally with great accuracy [6]. In the presence of superconducting (S) contacts this picture can be expected to change radically due to the different nature of the charge carriers.

For mesoscopic transport processes involving S leads, the energy-dependent quasiparticle (QP) spectrum has a gap Δ, which strongly inhibits tunneling at low energies and small τ [7]. At larger τ, multiparticle superconductive transport (MST) [7–9] comes into play. These processes can be either coherent, in the form of Josephson transport of Cooper pairs (CPs) without voltage drop, or they may be dissipative, as multiple Andreev reflection (MAR) of order m, which sets in above a bias voltage threshold $eV = 2\Delta/m$. Importantly, while MAR is itself dissipative and therefore incoherent, the transfer of m charges involved in such a MAR is a coherent tunneling process.

From the above discussion, it is clear that MST and CQ are antagonistic processes. On the one hand, CQ effects should deeply modify the energy thresholds for a m-particle tunneling process. On the other hand, MST could overthrow the CQ conditions known from the case of normal leads.

In this Letter, we address the delicate interplay of CQ and MST. We built a superconductor–superconductor–normal-metal (SSN)-SET by connecting in series a SS break junction (BJ) with a SN tunnel barrier (TB) and a capacitively coupled gate electrode (Fig. 1), providing thus the conditions for CQ in the S island between the BJ and the TB [3,4]. In the limit of a small total transmission $\mathcal{T}_{BJ} = \Sigma_i \tau_{i,BJ} \ll 1$ of the BJ, we study how the extra energy cost arising from CB affects the conductance thresholds for the different MAR processes. Furthermore,

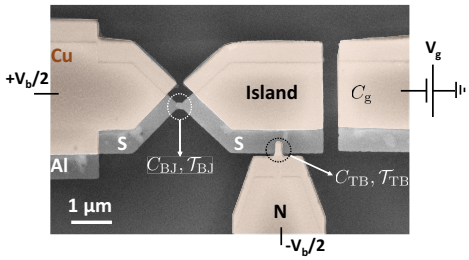

FIG. 1. Scanning electron microscope picture of a SET with a break junction (BJ) as one of the tunnel junctions in series with a superconductor–insulator-normal-metal tunnel barrier (TB), and the area in the middle (island) being capacitively coupled to a gate electrode.

in the limit of a larger $\mathcal{T}_{\mathrm{BJ}} \sim 1$, we observe that CQ enters in competition with the Josephson effect across the BJ, leading to the suppression of CB at low bias, whereas it is restored beyond the Josephson switching current. Our data are well described by a rate equation approach including CB as well as MST.

The transport in the SET is characterized by current cycles composed of charge transfer processes through the individual junctions comprising different types and different number of charged particles [10]. The e cycle is a process that charges the island with one QP through one junction, and discharges it through the other junction with another QP, leaving the island in its initial charge state. AR and MAR cycles charge the island with m electron charges through one junction, and subsequent single-QP or (M)AR processes discharge the island through the other junction. The Josephson quasiparticle (JQP) cycle [11–14] is a coherent process in which a CP tunnels through one junction, and simultaneously one QP tunnels off through the other junction. The initial charge state is reached by a subsequent single-QP process. The JQP cycle is resonant, i.e., it appears as a peak in the current-bias voltage ($I - V_{\mathrm{b}}$) characteristics.

Studies on all-superconducting (SSS)-SETs in the weak coupling regime (two TBs in series) showed e, JQP and processes comprising 3 QPs [10]. Another realization using a tunable junction showed a multitude of current cycles difficult to identify [15]. Hence the SSN-SET studied here is chosen to enable MST predominantly through just the BJ, reducing the number of processes. While some theoretical studies on the SSN-SET exist [16,17] it has not been investigated experimentally before.

For forming the tunable junction we use the thin-film BJ technique [18]. The BJ consists of an Al bridge suspended above a flexible substrate: by bending the substrate it is possible to adjust contacts with arbitrary transmission $\mathcal{T}_{\mathrm{BJ}}$ from the tunnel regime $\mathcal{T}_{\mathrm{BJ}} \ll 1$ to atomic-size contacts with $\mathcal{T}_{\mathrm{BJ}} \gtrsim 1$ [19,20]. The TB with fixed resistance R_{TB} is formed by an $\mathrm{Al}_x\mathrm{O}_y$ layer between the S (Al) and the N (Cu) material and hosts many channels in parallel with very small transmission $\tau_i \ll 1$ [2]. The electrostatic energy necessary to charge the island is $\mathcal{E}(n_{\mathrm{g}}, n) = E_{\mathrm{C}}(n - n_{\mathrm{g}})^2$ where n is the excess charge (in units of e) of the island, n_{g} is the equivalent charge induced by the gate voltage, and $C = C_{\mathrm{BJ}} + C_{\mathrm{TB}} + C_{\mathrm{g}}$ the total capacitance of the island. These individual capacitances determine the potential division in the SET described by the capacitor divisor $\kappa_i = (C_i + C_{\mathrm{g}}/2)/C$. In this Letter, we discuss data taken on one sample with $E_{\mathrm{C}} = 63.9\ \mu\mathrm{eV}$ $(= 0.33\Delta)$, $C_{\mathrm{g}} = 0.04$ fF, $C_{\mathrm{BJ}} = 1.08$ fF $(\kappa_{\mathrm{BJ}} = 0.88)$, $C_{\mathrm{TB}} = 0.13$ fF $(\kappa_{\mathrm{TB}} = 0.12)$, $\mathrm{R}_{\mathrm{TB}} = 48.4\ \mathrm{k}\Omega$, and $\Delta = 192\ \mu\mathrm{eV}$. The sample preparation, parameters, and data on three other samples are given in the Supplemental Material [21] (Secs. I, III, and V).

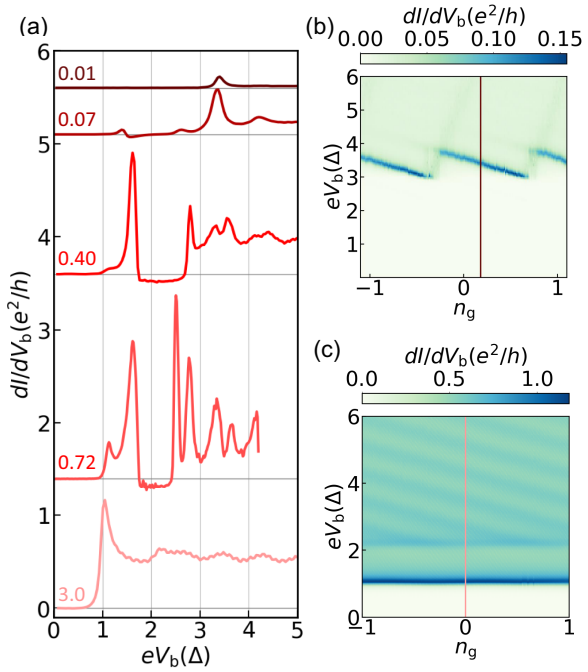

FIG. 2. Evolution of the transport processes measured in the SSN-SET for different $\mathcal{T}_{\mathrm{BJ}}$: (a) $\mathrm{d}I/\mathrm{d}V_{\mathrm{b}} - eV_{\mathrm{b}}$s for $\mathcal{T}_{\mathrm{BJ}} = 0.01$, 0.07, 0.40, 0.72, and 3 (from top to bottom). The datasets are offset vertically for clarity. The horizontal lines mark the x axes for the respective datasets. $n_{\mathrm{g}} - eV_{\mathrm{b}} - \mathrm{d}I/\mathrm{d}V_{\mathrm{b}}$ maps for $\mathcal{T}_{\mathrm{BJ}} = 0.01$ (b) and $\mathcal{T}_{\mathrm{BJ}} = 3$ (c).

Figure 2(a) shows $\mathrm{d}I/\mathrm{d}V_{\mathrm{b}} - eV_{\mathrm{b}}$ plots taken at fixed n_{g} for different $\mathcal{T}_{\mathrm{BJ}}$ (from top to bottom) of 0.01, 0.07, 0.4, 0.72, and 3. From these individual conductance curves we construct conductance–gate voltage–bias voltage ($n_{\mathrm{g}} - V_{\mathrm{b}} - \mathrm{d}I/\mathrm{d}V_{\mathrm{b}}$) maps. Two extreme examples, for $\mathcal{T}_{\mathrm{BJ}} = 0.01$ and 3, are given in Figs. 2(b) and 2(c). For the other transmissions, we plot the $n_{\mathrm{g}} - eV_{\mathrm{b}} - I$ in Figs. 3(a) and 3(b) ($\mathcal{T}_{\mathrm{BJ}} = 0.07$ and 0.4, respectively) and Fig. 4 for $\mathcal{T}_{\mathrm{BJ}} = 0.72$. The maps show that different current contributions are modulated by the gate voltage with e-periodicity with asymmetric slopes indicating different capacitances of the junctions. The positive or negative slope mark the onset of charge transport across the TB or BJ, respectively. The vertical red lines mark the n_{g} values at which the data in Fig. 2(a) have been taken. They correspond to positions in the middle of the descending slope of a CB diamond [25].

For $\mathcal{T}_{\mathrm{BJ}} = 0.01$ in Fig. 2(a), we observe only one peak at 3Δ, marking the e process. For $\mathcal{T}_{\mathrm{BJ}} = 0.07$, the peak corresponding to the e process is bigger in amplitude, and two additional peaks appear between Δ and 3Δ. The first one, located between $\Delta + E_{\mathrm{C}}$ and $\Delta + 3E_{\mathrm{C}}$ ($\sim 1.4\Delta$ and 2.2Δ), corresponds to a JQP cycle [10,13,15,26]. The second (with a lower threshold of $2\Delta + E_{\mathrm{C}}$) represents a cycle involving AR across the BJ. The peak at around 4.5Δ indicates the next step in the Coulomb staircase. For $\mathcal{T}_{\mathrm{BJ}} = 0.4$ the amplitude of the JQP and the AR cycle increase

further. At the position of the e process a double peak occurs that we identify as a combination of AR and MAR with $m = 3$. For $\mathcal{T}_{\mathrm{BJ}} = 0.72$ the amplitude of the MAR and JQP cycles has further increased such that the JQP of the adjacent diamond, i.e., signaling the next charge state, gives rise to the highest peak at around 2.4Δ. There is no peak at 3Δ, and all the features between 3Δ and $3\Delta + 2E_{\mathrm{C}}$ are smaller in amplitude than the peak starting at 2.4Δ. This means that for this transmission, cycles including MST are more relevant than e transport. Besides, there is a peak above Δ that can be explained by considering cotunneling of several QPs, see below. For large $\mathcal{T}_{\mathrm{BJ}}$ high Josephson currents can flow. In this situation the voltage drops completely across the TB, and the island's chemical potential remains pinned to that of the S contact. This is visible in the lowest trace in Fig. 2(a) as well as in Fig. 2(c), where between Δ and 2.2Δ no gate dependence is observed, indicating a suppression of CB. Upon further increasing $|eV_{\mathrm{b}}|$ to about 2.2Δ, gate-dependent conductance features with the same slope and the same periodicity as observed for small $\mathcal{T}_{\mathrm{BJ}}$ reappear. As the dissipation-free state of the SS junction is lost, the island's potential is no longer pinned to that of the S lead. Consequently, the SS junction switches from vanishing to high impedance. We posit that this transition restores the CB effects despite the large $\mathcal{T}_{\mathrm{BJ}} \approx 3$. At this threshold, in the given example the switching current amounts to $I_{\mathrm{s}} = 7.0$ nA and is hence about an order of magnitude below the nominal I_{c} for a tunnel junction, estimated as $I_{\mathrm{c}} = (\pi/2)G_0\tau\Delta \approx 69$ nA [27]. Such a reduction of I_{s} with respect to I_{c} is generic in junctions with Josephson energy $E_J \sim E_c$, and in agreement with reports from earlier experimental [28,29] and theoretical works [30] in SSS-SETs. Related data is presented in Fig. S8 and described in Sec. X in the Supplemental Material [21].

To verify this assignment of the various contributions, we calculate the current through the device with the rate equation approach [Eq. (2)] [1]. We take into account the JQP rate $\Gamma_{\mathrm{JQP}}(\delta E)$ from Averin and Aleshkin [31] and rates derived from the full counting statistics for (M)AR processes $\Gamma_{\mathrm{MAR}}(\delta E)$ [32] in the BJ. For the TB, we solely use the classical rate expression for a SN junction [7,33]. Detailed information regarding the rates and parameters is given in Sec. IV of the Supplemental Material [21]. The electrostatic energy difference can be expressed as [1]

$$\delta E = \mathcal{E}(n_{\mathrm{g}}, n) - \mathcal{E}(n_{\mathrm{g}}, n + n') + n'\kappa_i eV_{\mathrm{b}}, \qquad (1)$$

where n' is the number of transferred charges. We assume that there is no accumulation of electrons in the island or relevant environment and neglect effects of the environment [34], so $dP/dt = 0$ and the current through the two junctions is equal. Considering the normalization condition $\sum_n P_n = 1$ we solve the stationary rate equation

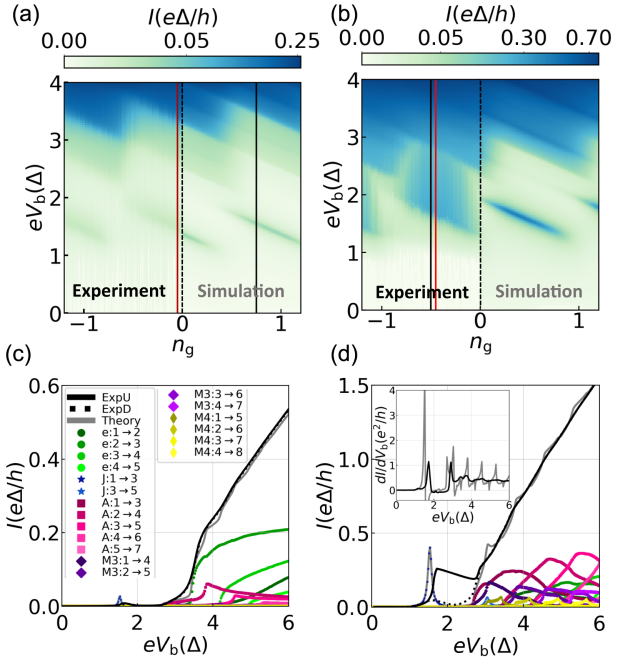

FIG. 3. Theoretical and experimental $n_{\mathrm{g}} - eV_{\mathrm{b}} - I$ maps for a contact with $\mathcal{T}_{\mathrm{BJ}} = 0.07$ (a) and $\mathcal{T}_{\mathrm{BJ}} = 0.4$ (b). Red lines in (a) and (b) mark the n_{g} positions at which the $\mathrm{d}I/\mathrm{d}V_{\mathrm{b}}$ data of Fig. 2(a) have been taken. (c),(d): corresponding $I - eV_{\mathrm{b}}$s as marked in (a) and (b) with solid black lines. Black: experiment (solid or dashed line: increasing or decreasing $|V_{\mathrm{b}}|$). Gray: simulation. Scatter plots: $P_n\Gamma_{n\to n+n'}$ contributions (with amplitude $> 0.05e\Delta/h$): e (e: $n \to n+1$, green), AR (A: $n \to n+2$, pink), $m = 3$ MAR (M3: $n \to n+3$, purple), $m = 4$ MAR (M4: $n \to n+4$, yellow). Inset in (d): experimental (black) and simulated (gray) $\mathrm{d}I/\mathrm{d}V_{\mathrm{b}}$.

$$\sum_{n'\neq 0} P_{n+n'}\Gamma_{n+n'\to n} - P_n \sum_{n'\neq 0} \Gamma_{n\to n+n'} = 0 \qquad (2)$$

and obtain the probabilities P_n. With these we calculate the total current by considering the charge transferred through the BJ,

$$I = (-e) \sum_{n;n'\neq 0} \tilde{n}\, P_n \Gamma_{\mathrm{BJ},n\to n+n'}. \qquad (3)$$

Here, n' can also be negative, and $\tilde{n}$ is the charge transferred in the BJ (which may be different from n').

Figures 3(a) and 3(c) are the $n_{\mathrm{g}} - eV_{\mathrm{b}} - I$ map and a $I - eV_{\mathrm{b}}$ trace at $n_{\mathrm{g}} = 0.75$ as indicated in the map, for $\mathcal{T}_{\mathrm{BJ}} = 0.07$. In Fig. 3(c), the black (gray) lines correspond to experimental (calculated) curves (solid or dotted for increasing or decreasing voltage). The colored symbols depict the individual contributions $P_n\Gamma_{n\to n+n'}$ that sum up to the total current. The resonant peak in the experiment follows the JQP contribution from the simulation, and the feature starting at 2.4Δ is due to a cycle with AR [10,35]. Figures 3(b) and 3(d) show the comparison of experiment and theory for $\mathcal{T}_{\mathrm{BJ}} = 0.4$. As Fig. 3(b) shows, the subgap

current $|eV_b| < 3\Delta$ becomes more pronounced and there is almost no color change at 3Δ. A detailed analysis in Sec. VIII and Fig. S7 in the Supplemental Material [21] shows that a quantitative agreement between the experimental and simulated current can only be obtained when JQP, AR, and MAR processes are taken into account. We note that since at $\mathcal{T}_{BJ} = 0.4$ we can assume a single channel with $\tau_{BJ} = 0.4$ and which also fixes the slope of the IV_b, there is no free fit parameter. Instead, all parameters used in the simulation can be determined independently from other opening states of the BJ and the normal state map. The large blue area in the experimental map above the JQP line (above $\sim 1.5\Delta$) is a result of the resonant character of the JQP and is absent for the down sweep (see Supplemental Material [21], Secs. VI, IX, and XI). The decomposition into individual cycles in Fig. 3(d) (see also Fig. S7 and Sec. VIII in the Supplemental Material [21]) confirms that AR and MAR with $m = 3$ (pink and purple symbols) are bigger in amplitude than the e transport (green symbols). In single SS junctions e and AR persist to very high bias, while MAR fades out above 2Δ [32]. In contrast, here, MAR contributes also to the current far outside the gap region suggesting that MAR processes become more robust by the interplay with CB. The dI/dV_b in the inset shows that the multi-peak characteristic of each charge state found in the simulation, indicative for the presence of the MAR processes (Fig. S7 in the Supplemental Material [21]), is also observed in the experimental curve, yet rounded due to the finite measurement T [36].

For even higher $\mathcal{T}_{BJ}$ (Fig. 4) the amplitudes of the processes setting in below 3Δ increase, and a new line appears at $|eV_b| = \Delta$. In the $n_g - eV_b$ map the slope of this cycle is around 3 times smaller than the one of the other cycles. This feature appears as a peak at $\sim\Delta$ in the dI/dV_b curve, see Figs. 4 and 2. This consists of a coherent tunneling process that simultaneously transports three elementary charges through the BJ and two through the TB, hence implies AR in the TB, hence called 5QP process. The electrostatic energy balance $\delta E = \mathcal{E}(n_g, n) - \mathcal{E}(n_g, n+1) + (3\kappa_{BJ} + 2\kappa_{TB})eV_b$ implies that the island charge changes by e and that the slope in the $n_g - eV_b$ map is a function of the capacitance ratio and the number of charge carriers involved (in this case $1/2.88$, so close to $1/3$) [37,38]. The expression for the rate of such a 5QP process has not been worked out theoretically. Therefore, we model the rate as a step function starting at $\delta E = 2\Delta$ with an amplitude as free parameter that was determined by fitting to $0.015\ s^{-1}$. In Fig. 4 we show the comparison between experiment and theory for the contact with $\mathcal{T}_{BJ} = 0.72$ that shows this feature starting at $|eV_b| = \Delta$ and with a slope in agreement with the experimental result. The contributions at higher bias, namely the JQP and MAR cycles, appear in the simulation at around the same position as in the experimental map. The amplitude of both

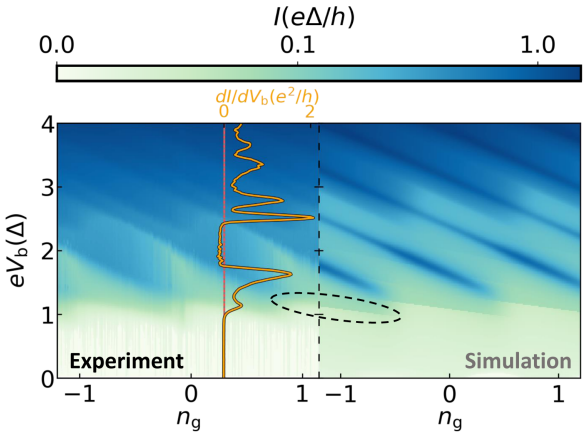

FIG. 4. Experimental and simulated maps for $\mathcal{T}_{BJ} = 0.72$. The red line marks the position at which the line cut shown in Fig. 2(a) has been taken. The dashed line highlights the current onset with slope $\sim 1/3$ compared to the CB diamond edges. This feature at $\sim\Delta$ as well as the double-peak feature at larger voltages are also visible in the superimposed dI/dV_b vs V_b plot.

processes overcomes the e transport for high voltages and extends to very high $|V_b|$. The double line above 2.5Δ is the result of JQP and MAR cycles from different initial charge states of the island. We note that we also included the 3QP process (AR in the BJ and e in the TB) in the simulation with a rate with amplitude $0.02\ s^{-1}$. This contribution sets in at $eV_b \sim 1.5\Delta$, has a slope of $\sim 1/2$ and its onset is therefore hidden by the JQP contribution but nevertheless markedly improves the agreement between theory and experiment. Further discussion and simulations regarding the 3QP and the 5QP processes are shown in Sec. XI and Fig. S9 of the Supplemental Material [21].

In conclusion, we presented transport properties of a tunable SSN-SET varying the relative strength of e, JQP, AR, and MAR processes to show the mutual influence between MST processes and CQ. While in single junctions MAR processes are not relevant outside the gap region, the presence of CQ enhances the contributions of MAR at high bias. The description based on charge states of the island allows to reproduce the experimental data up to relatively strong coupling $\mathcal{T}_{BJ} \simeq 1$ when taking also MAR cycles into account. For higher $\mathcal{T}_{BJ}$, cotunneling events that also include AR and MAR become relevant. We observe the reappearance of charging effects at high bias in the strong coupling regime ($\mathcal{T}_{BJ} > 1$, when at least one channel with a transmission $\tau = 1$ exists in the BJ [19,39–41], while at low bias and in the normal-conducting state all signature of CQ has already disappeared. Our findings are important for designing and understanding nanoscale superconducting quantum devices, such as superconducting qubits [42], with arbitrary intermediate transmissions to use the subtle interplay between the charge and phase degrees of freedom as a resource for optimizing their performance.

We thank J. C. Cuevas for fruitful discussion and S. Sprenger and T. Lorenz-Sprenger for experimental support.

We acknowledge the use of the experimental equipment and the expert support concerning its usage provided by the Nanostructure Laboratory at the University of Konstanz. We gratefully acknowledge funding by the European Commission through the Marie Skłodowska-Curie Grant Agreement No. 766025 (QuESTech) and the Deutsche Forschungsgemeinschaft (DFG; German Research Foundation) by SFB 1432 (Project No. 425217212). J. S. was supported by Grant PID2021-126273NB-I00 funded by MCIN/AEI/10.13039/501100011033 and by "ERDF A way of making Europe" as well as by the Basque Government through Grant No. IT1470-22.

*elke.scheer@uni-konstanz.de

[1] *Single Charge Tunneling*, edited by H. Grabert and M. H. Devoret (Springer, Boston, MA, 1992).
[2] Y. Nazarov and Y. Blanter, *Quantum Transport* (Cambridge University Press, Cambridge, England, 2009).
[3] K. Likharev, Single-electron transistors: Electrostatic analogs of the dc SQUIDs, IEEE Trans. Mag. **23**, 1142 (1987).
[4] T. A. Fulton and G. J. Dolan, Observation of single-electron charging effects in small tunnel junctions, Phys. Rev. Lett. **59**, 109 (1987).
[5] Y. V. Nazarov, Coulomb blockade without tunnel junctions, Phys. Rev. Lett. **82**, 1245 (1999).
[6] S. Jezouin, Z. Iftikhar, A. Anthore, F. D. Parmentier, U. Gennser, A. Cavanna, A. Ouerghi, I. P. Levkivskyi, E. Idrisov, E. V. Sukhorukov, L. I. Glazman, and F. Pierre, Controlling charge quantization with quantum fluctuations, Nature (London) **536**, 58 (2016).
[7] M. Tinkham, *Introduction to Superconductivity* 2nd ed. (McGraw-Hill International Editions, New York, 1996).
[8] G. E. Blonder, M. Tinkham, and T. M. Klapwijk, Transition from metallic to tunneling regimes in superconducting microconstrictions: Excess current, charge imbalance, and supercurrent conversion, Phys. Rev. B **25**, 4515 (1982).
[9] B. Pannetier and H. Courtois, Andreev reflection and proximity effect, J. Low Temp. Phys. **118**, 599 (2000).
[10] R. J. Fitzgerald, S. L. Pohlen, and M. Tinkham, Observation of Andreev reflection in all-superconducting single-electron transistors, Phys. Rev. B **57**, R11073 (1998).
[11] D. V. Averin and K. K. Likharev, Coulomb blockade of single-electron tunneling, and coherent oscillations in small tunnel junctions, J. Low Temp. Phys. **62**, 345 (1986).
[12] Y. Nakamura, C. D. Chen, and J. S. Tsai, Quantitative analysis of Josephson-quasiparticle current in superconducting single-electron transistors, Phys. Rev. B **53**, 8234 (1996).
[13] S. L. Pohlen, R. J. Fitzgerald, and M. Tinkham, The Josephson–quasiparticle (JQP) current cycle in the superconducting single-electron transistor, Physica (Amsterdam) **284-288B**, 1812 (2000).
[14] A. J. Manninen, Y. A. Pashkin, A. N. Korotkov, and J. P. Pekola, Observation of thermally excited charge transport modes in a superconducting single-electron transistor, Europhys. Lett. **39**, 305 (1997).
[15] T. Lorenz, S. Sprenger, and E. Scheer, Coulomb blockade and multiple Andreev reflection in a superconducting single-electron transistor, J. Low Temp. Phys. **191**, 301 (2018).
[16] F. W. J. Hekking, L. I. Glazman, and G. Schön, Andreev spectroscopy of Josephson coupling, Phys. Rev. B **51**, 15312 (1995).
[17] R. Fazio, G. Schön, and J. Siewert, Current–voltage characteristics of NSS transistors, Physica (Amsterdam) **284-288B**, 1828 (2000).
[18] J. van Ruitenbeek, A. Alvarez, I. Piñeyro, C. Grahmann, P. Joyez, M. H. Devoret, D. Esteve, and C. Urbina, Adjustable nanofabricated atomic size contacts, Rev. Sci. Instrum. **67**, 108 (1996).
[19] E. Scheer, P. Joyez, D. Esteve, C. Urbina, and M. H. Devoret, Conduction channel transmissions of atomic-size aluminum contacts, Phys. Rev. Lett. **78**, 3535 (1997).
[20] N. Agraït, A. L. Yeyati, and J. M. van Ruitenbeek, Quantum properties of atomic-sized conductors, Phys. Rep. **377**, 81 (2003).
[21] See Supplemental Material at http://link.aps.org/supplemental/10.1103/PhysRevLett.132.057001 for experimental and simulation details as well as additional experimental and simulation data including Refs. [22–24].
[22] T. Lorenz, Wechselspiel von Vielteilchen-Transport und Ladungseffekten in supraleitenden Einzelelektronentransistoren, Ph.D. thesis, Universität Konstanz, Konstanz, 2018.
[23] R. C. Dynes, V. Narayanamurti, and J. P. Garno, Direct measurement of quasiparticle-lifetime broadening in a strong-coupled superconductor, Phys. Rev. Lett. **41**, 1509 (1978).
[24] J. C. Cuevas and W. Belzig, dc transport in superconducting point contacts: A full-counting-statistics view, Phys. Rev. B **70**, 214512 (2004).
[25] We show here data for positive V_b, but note that all maps were symmetric with respect to the bias polarity when choosing the adequate n_g. For intermediate $\mathcal{T}_{BJ} \sim 0.5$ the peak slightly above Δ is hysteretic with respect to the bias sweep direction; see Sec. VI of the Supplemental Material [21].
[26] Y. Nakamura, T. Sakamoto, and J. S. Tsai, Study of Josephson-quasiparticle cycles in superconducting single-electron transistors, Jpn. J. Appl. Phys. **34**, 4562 (1995).
[27] V. Ambegaokar and A. Baratoff, Tunneling between superconductors, Phys. Rev. Lett. **10**, 486 (1963).
[28] P. Joyez, P. Lafarge, A. Filipe, D. Esteve, and M. H. Devoret, Observation of parity-induced suppression of Josephson tunneling in the superconducting single electron transistor, Phys. Rev. Lett. **72**, 2458 (1994).
[29] J.-P. Cleuziou, W. Wernsdorfer, V. Bouchiat, T. Ondarçuhu, and M. Monthioux, Carbon nanotube superconducting quantum interference device, Nat. Nanotechnol. **1**, 53 (2006).
[30] A. Maassen van den Brink, G. Schön, and L. J. Geerligs, Combined single-electron and coherent-Cooper-pair tunneling in voltage-biased Josephson junctions, Phys. Rev. Lett. **67**, 3030 (1991).
[31] D. V. Averin and V. Y. Aleshkin, Resonance tunneling of Cooper pairs in a system of two small Josephson junctions, JETP Lett. **50**, 367 (1989).
[32] J. C. Cuevas and W. Belzig, Full counting statistics of multiple Andreev reflections, Phys. Rev. Lett. **91**, 187001 (2003).

[33] For describing the cotunneling processes at intermediate coupling we also take a small AR contribution through the TB into account.

[34] J. P. Pekola, V. F. Maisi, S. Kafanov, N. Chekurov, A. Kemppinen, Y. A. Pashkin, O.-P. Saira, M. Möttönen, and J. S. Tsai, Environment-assisted tunneling as an origin of the Dynes density of states, Phys. Rev. Lett. **105**, 026803 (2010).

[35] V. F. Maisi, O. P. Saira, Y. A. Pashkin, J. S. Tsai, D. V. Averin, and J. P. Pekola, Real-time observation of discrete Andreev tunneling events, Phys. Rev. Lett. **106**, 217003 (2011).

[36] We note that Al single-atom contacts with $\mathcal{T} \gtrsim 0.8$ are expected to accommodate more than one channel [19]. For this contact with $\mathcal{T} = 0.4$ it was sufficient to consider one single channel with $\tau = 0.4$. Considering more than one channel would result in a smaller current, and hence, would not improve the agreement between experiment and simulation. Furthermore, we tried to reproduce the experimental IV_b without MAR by using different values of Δ, R_{TB}, E_C, and/or κ, but failed.

[37] P. Joyez, Le transistor a une paire de Cooper: Un système quantique macroscopique, Ph.D. thesis, Université Paris 6, CEA-Saclay, 1995.

[38] J. Siewert and G. Schön, Charge transport in voltage-biased superconducting SET transistors, Phys. Rev. B **54**, 7421 (1996).

[39] M. L. Della Rocca, M. Chauvin, B. Huard, H. Pothier, D. Esteve, and C. Urbina, Measurement of the current-phase relation of superconducting atomic contacts, Phys. Rev. Lett. **99**, 127005 (2007).

[40] L. Bretheau, Ç. Ö. Girit, C. Urbina, D. Esteve, and H. Pothier, Supercurrent spectroscopy of Andreev states, Phys. Rev. X **3**, 041034 (2013).

[41] J. Senkpiel, R. Drost, J. C. Klöckner, M. Etzkorn, J. Ankerhold, J. C. Cuevas, F. Pauly, K. Kern, and C. R. Ast, Extracting transport channel transmissions in scanning tunneling microscopy using superconducting excess current, Phys. Rev. B **105**, 165401 (2022).

[42] I. Siddiqi, Engineering high-coherence superconducting qubits, Nat. Rev. Mater. **6**, 875 (2021).